Eur. J. Mineral.
2005, **17**, 411–421

A comparative study of fibrous zeolites under pressure

GIACOMO DIEGO GATTA

Dipartimento di Scienze della Terra, Università degli Studi di Milano, Via Botticelli 23, I-20133 Milano, Italy
e-mail: diego.gatta@unimi.it

Abstract: Fibrous zeolites (FZ) are the only group of natural zeolites that have been well investigated under pressure. The high-pressure (H*P*) behaviour of several FZ has been studied by means of *in situ* H*P*-single-crystal/powder diffraction experiments. Here I report a comparative study on lattice compressibility, structural deformation mechanisms and the role played by the framework (Si/Al-distribution, cross-linking of the building unit chains) and extra-framework content on the H*P*-behaviour of FZ. The structural analogy among the FZ group, due to the 4 = 1 secondary building unit (SBU), induces similar elastic behaviour and a "FZ-average bulk modulus" can be calculated: $K_{T0} = 50 \pm 10$ GPa. The bulk modulus value changes as function of the extra-framework content, following the sequence: K_{T0}(Ba-FZ)>K_{T0}(Ca-FZ)>K_{T0}((Ca+Na)-FZ)>K_{T0}(Na-FZ). Another interesting result is related to the axial compressibility. The experiments on natrolite, scolecite, edingtonite and thomsonite show that the elastic anisotropy, represented by the axial bulk moduli, is strongly influenced by the tetragonal topological symmetry. The H*P*-structural refinements performed show one main deformation mechanism for all these zeolites: the cooperative rotation (anti-rotation) of the SBU. This mechanism strongly reduces the free volume of the 8-membered ring channels, parallel to the SBU-chain direction.

Key-words: fibrous zeolites, high-pressure, comparative compressibility, isothermal equations-of-state.

Introduction

Physical and chemical properties of open-framework materials make natural and synthetic micro- and mesoporous silicates, phosphate, sulphide and selenides an object of attention for their advanced technological applications (Li *et al.*, 1999; Kallo, 2001; Tchernev, 2001; Davis, 2002; Zheng *et al.*, 2002; Bish *et al.*, 2003; Zheng *et al.,* 2003; Lee *et al.,* 2004a). Thermal transformations, catalytic properties, cation-exchange activity, ionic conductivity and photoluminescent features have been investigated extensively. In contrast, the *P*-induced structural modifications and the elastic properties of these materials are not well known. A few studies have been dedicated to natural zeolites under pressure and the majority of them to the "fibrous zeolite" group.

Lee *et al.* (2002a and b) have investigated the behaviour of natrolite under pressure, and natrolite-analogues, by means of *in situ* synchrotron powder diffraction. The authors showed a *P*-induced over-hydration effect between 0.8-1.5 GPa, through the selective sorption of water molecules from the hydrostatic pressure fluid (a mixture of methanol:ethanol:water) into the structural channels.

Ballone *et al.* (2002) and Comodi *et al.* (2002) studied the H*P*-behaviour of scolecite by means of *in situ* synchrotron powder diffraction and single-crystal X-ray diffraction, respectively. Using a non-penetrating pressure medium, scolecite does not undergo a phase transition, at least up to 5 GPa (which is the maximum pressure achieved during the single-crystal experiment). However, Ballone *et al.* (2002) reported an anomalous elastic behaviour of scolecite at *P*>5 GPa, in a pressure range not investigated by single-crystal diffraction.

Gatta *et al.* (2004a) studied the elastic response of tetragonal edingtonite under pressure by means of single-crystal X-ray diffraction data using a non-penetrating pressure fluid, defining the isothermal equation-of-state (EoS) and describing the main deformation mechanism of framework and extra-framework content. Lee *et al.* (2004b) reported the elastic behaviour of orthorhombic edingtonite and thomsonite by *in situ* synchrotron powder diffraction. Finally, Gatta *et al.* (2004b) studied the comparative compressibility of orthorhombic and tetragonal edingtonite on the basis of single-crystal diffraction data using a nominally penetrating pressure medium.

The aim of this study is to compare the elastic behaviour of the aforementioned fibrous zeolites on the basis of the previous experimental data, in order to define the role played by: i) the Si/Al-ordering, ii) the different cross-linking of the "building block unit" chains, iii) the extra-framework content (nature of the cations and ionic valence, ionic radii, coordination number) on the *P*-behaviour of the FZ. In addition, the comparison of H*P*-structural refinements is useful to define the main deformation mechanisms for this group of zeolites. Moreover, a comparison between pressure and thermal-induced structural modification of fibrous zeolites is carried out.

0935-1221/05/0017-0411 $ 4.95
DOI: 10.1127/0935-1221/2005/0017-0411

Crystal structure of the fibrous zeolites investigated under pressure

The crystal structure of "fibrous zeolites" is built on the 4 = 1 "secondary building units" (SBU, Gottardi & Galli, 1985; Armbruster & Gunter, 2001; Berlocher *et al.*, 2001). These building block units, also know as "T_5O_{10} tetrahedral units", form chains running along [001], with tetragonal topological symmetry (Fig. 1). Smith (1983) showed the different possible combinations of the chains and reported that three of them correspond to natural fibrous zeolites: edingtonite, natrolite and thomsonite. The different connectivity pattern of the chains in edingtonite, natrolite and thomsonite is shown in Fig. 1. The edingtonite framework is the simplest, without any relative translation between the linked chains. In the natrolite framework, the chains are mutually translated along [001] of ±1/4*c* (about 1.65 Å, Fig. 1). Every chain is translated with respect to its four nearest neighbours and such translations are evident on both (100) and (010)-planes (or more simply viewing the projections of the structure perpendicular to the planes (110) and (1$\bar{1}$0), Fig. 1). The thomsonite framework also shows a mutual translation of the [001]-chains (with a relative shift of about 1.65 Å) but the cross-linking geometry is different from natrolite: the translation is evident only on the (010)-plane, and not on the (100)-plane (Armbruster & Gunter, 2001). The topological configuration of the three framework types (EDI, NAT and THO, Baerlocher *et al.*, 2001) appears to be very similar viewed down to [001] (Fig. 2). All the fibrous zeolites show two different systems of channels: 8-membered ring channels running along the [001] and 8-membered ring channels running along the [110] in edingtonite, [110] in natrolite and [010] in thomsonite.

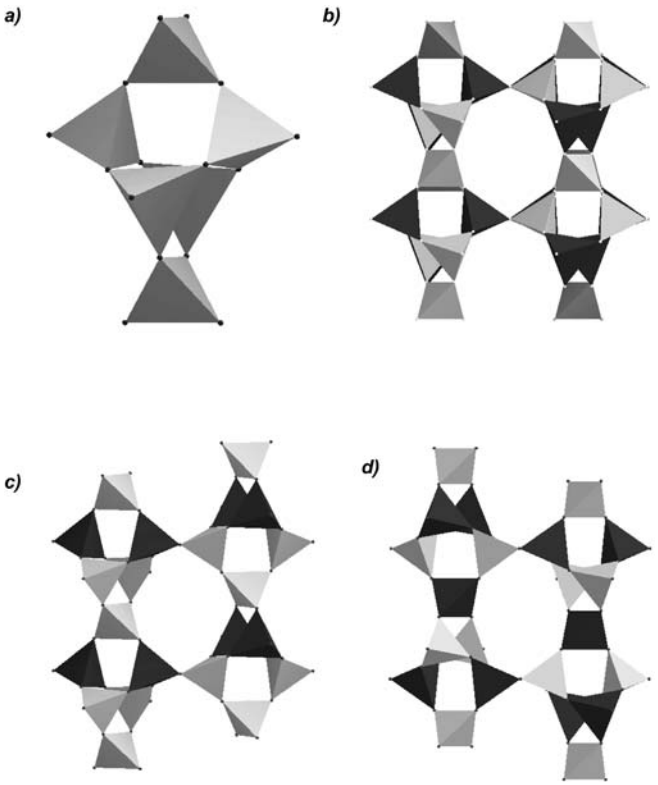

Fig. 1. Topological configuration of the fibrous zeolites framework. *a*) 4 = 1 secondary building unit. *b*) Cross linking of the SBU-chains of edingtonite viewed perpendicular to (110), *c*) of natrolite viewed perpendicular to (110) and *d*) of thomsonite viewed perpendicular to (010). Si-tetrahedra are represented in light-grey, whereas Al-tetrahedra in dark-grey.

Different degrees of Si/Al-ordering and extra-framework content make the crystal-chemistry of this zeolite group complex. Edingtonite is a Ba-fibrous zeolite, of nominal composition $Ba_2Al_4Si_6O_{20}\cdot 8H_2O$, which shows two isomorphic crystal structures characterised by a different Si/Al-distribution: tetragonal ($P\bar{4}2_1m$), with a complete Si/Al-disorder in the tetrahedral sites (Mazzi *et al.,* 1984); orthorhombic ($P2_12_12$), with complete Si/Al-ordering (Galli, 1976; Gatta & Boffa Ballaran, 2004). Natrolite is an Na-fibrous zeolite, ideal composition $Na_{16}Al_{16}Si_{24}O_{80}\cdot 16H_2O$, characterised by an almost fully ordered Si/Al-arrangement (Artioli *et al.*, 1984). Disordered sample have also been found (Alberti & Vezzalini, 1981; Krogh Andersen *et al.*, 1990). Two other isotypic fibrous zeolites belonging to the natrolite subgroup are: scolecite ($Ca_8Al_{16}Si_{24}O_{80}\cdot 24H_2O$, *Cc*, Comodi *et al.*, 2002) and mesolite ($Na_{16}Ca_{16}Al_{48}Si_{72}O_{240}\cdot 64H_2O$, *Fdd*2, Artioli *et al.*, 1996; Stukkenschmidt & Kirfel, 2000). Scolecite and mesolite display almost complete Si/Al-ordering. It is useful to note that the crystal structure of scolecite has been refined in two different space groups: the non-conventional *F*1*d*1 (Fälth & Hansen, 1979) and the standard *Cc* space group (Comodi *et al.*, 2002). In the latter case, the 4 = 1 SBU-chains run along the [100]-axis. Thomsonite, ideal composition $Na_4Ca_8Al_{20}Si_{20}O_{80}\cdot 24H_2O$ (*Pncn*, Alberti *et al.*, 1981; Ståhl *et al.*, 1990), is a completely Si/Al-ordered zeolite.

The extra-framework content of the aforementioned zeolites, represented by monovalent and/or bivalent large cations and water molecules, lies in the 8-membered ring channel along [001]. Natrolite accommodates, into the [001]-channels, two Na-sites and two H_2O-sites (Fig. 2b). The extra-framework content of scolecite is represented by one Ca-site and three H_2O-sites (Fig. 2c). Mesolite shows two distinct channels types: one accommodates two Na-sites and two H_2O-site (as in the natrolite structure), and the other accommodates one Ca-site and three H_2O-site (as in the scolecite structure) (Fig. 2d). Due to the Na/Ca ordering in the channels, mesolite displays a super-lattice with the *b*-axis three times that of natrolite. Also for thomsonite, the extra-framework content lies in two distinct channel types with different arrangements: a fully occupied site, with either Na or Ca in equal amounts, resides in one channel type; two split sites (only 0.5 Å apart) partially occupied by Ca lie in the other channel type. Four H_2O-sites can been located, two of them in the channel where (Na,Ca)-sites are, and the other two closer to the channel-edge (Fig. 2e). Edingtonite shows only one Ba-site located on the two-fold (or four-fold) axis, found to be split into two sites, only 0.3-0.4 Å apart (Mazzi *et al.*, 1984; Gatta & Boffa Ballaran, 2004), and two independent water molecule sites, one close to the center of the [001]-channel and one close to the channel's edge. The Ba-polyhedron is ten-fold coordinated: four oxygen's belonging to the framework and six oxygen's belonging to the H_2O-molecules (Fig. 2a). Since the shape and the free volume of the [001]-channels are influenced by the cross-link-

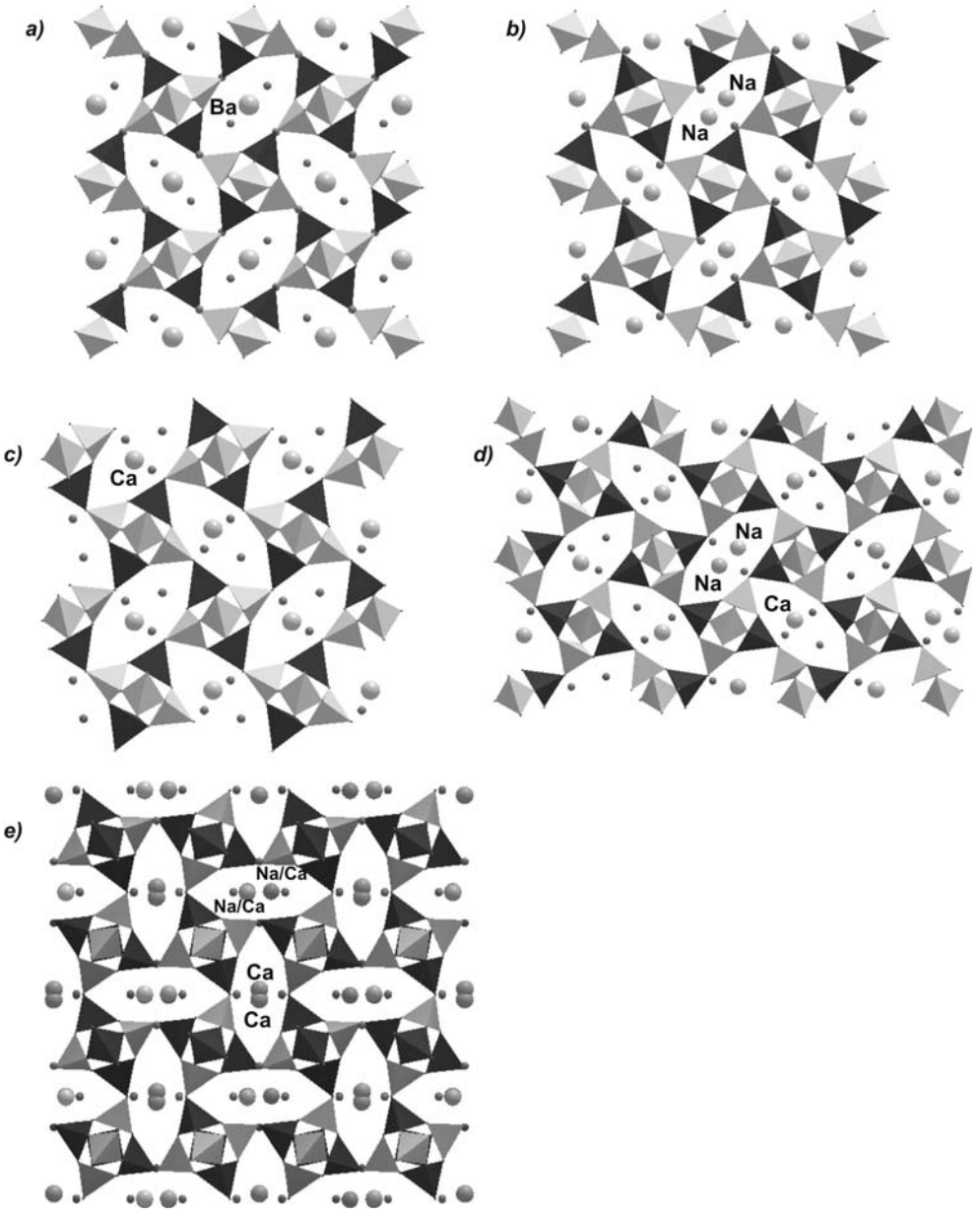

Fig. 2. Projections of the fibrous zeolites structure on the plane perpendicular to the SBU-chains: *a)* edingtonite, *b)* natrolite, *c)* scolecite, *d)* mesolite and *e)* thomsonite. Si-tetrahedra are represented in light-grey, whereas Al-tetrahedra in dark-grey. For the extra-framwork content, the small spheres represent the oxygens of the water molecules, whereas the large ones represent monovalent/divalent cations.

ing of the SBU-chains, the crystal structure of edingtonite is characterised by the largest channels with respect to the other fibrous zeolites. Thus, large cations (e.g. Ba, Sr, Ca) preferably reside in the channels of edingtonite.

More details on the crystal structure, crystal chemistry, thermal and other physico-chemical properties, occurrences and genesis of natural fibrous zeolites can be found in Gottardi & Galli (1985), Armbruster & Gunter (2001), Passaglia & Sheppard (2001).

H*P*-experiments: *in situ* single-crystal and powder diffraction

The H*P*-studies of fibrous zeolites presented here were conducted by means of *in-situ* single-crystal diffraction and synchrotron powder diffraction.

The *P*-behaviour of scolecite and edingtonite (orthorhombic and tetragonal) have been studied using single-crystal X-ray diffraction data with a common Merrill-Basset diamond anvil cell (DAC) (Merrill & Bassett, 1974) and a BGI-DAC (Allan *et al.*, 1996), respectively. Only the experiments on scolecite were conducted with a non-penetrating pressure transmitting medium (silicon-oil) and up to 4.21 GPa. The pressure was measured using the Sm^{2+}:BaFCl fluorescence method (Comodi & Zanazzi, 1993); the uncertainties in the pressure measurements were ± 0.05 GPa. The *P*-induced structural evolution of edingtonite was studied using both non-penetrating pressure transmitting medium (glycerol, Gatta *et al.*, 2004a) up to 5.08 GPa and nominally penetrating medium (methanol:ethanol:water = 16:3:1, Gatta *et al.*, 2004b) up to 6.74 GPa. The pressure was calibrated by detecting the shift in the R1 emission line of the included ruby chips (Mao *et al.*, 1986), with deviations in the mea-

Table 1. Cell parameters of natrolite (after Lee *et al.*, 2002a), scolecite (after Comodi *et al.*, 2002), orthorhombic-tetragonal edingtonite (after Gatta *et al.*, 2004b) and thomsonite (after Lee *et al.*, 2004b).

P (GPa)	*a* (Å)	*b* (Å)	*c* (Å)	β (°)	*V* (Å^3)
Natrolite					
0.0001	–	–	–	–	–
0.40(10)	18.226(2)	18.583(2)	6.579(1)	–	2228.2(5)
0.84(10)	18.180(4)	18.531(4)	6.566(2)	–	2212.0(8)
1.51(10)	18.390(6)	18.829(6)	6.547(2)	–	2267.0(10)
1.72(10)	18.378(3)	18.818(3)	6.545(1)	–	2263.5(6)
2.42(10)	18.233(3)	18.679(3)	6.530(1)	–	2223.9(6)
3.58(10)	18.097(2)	18.518(2)	6.512(1)	–	2182.3(5)
5.01(10)	17.924(2)	18.325(2)	6.487(1)	–	2130.7(5)
Scolecite					
0.0001	6.533(2)	19.030(3)	9.830(3)	109.95(3)	1148.76(4)
0.37(5)	6.518(3)	18.986(4)	9.790(3)	109.93(3)	1138.96(5)
0.64(5)	6.513(3)	18.961(4)	9.785(3)	109.89(3)	1136.29(5)
0.95(5)	6.499(3)	18.894(4)	9.761(4)	109.88(4)	1127.14(6)
1.52(5)	6.478(4)	18.871(6)	9.730(4)	109.80(4)	1119.14(6)
1.77(5)	6.471(4)	18.804(5)	9.723(5)	109.79(6)	1113.23(6)
2.63(5)	6.451(5)	18.761(6)	9.683(5)	109.67(5)	1103.52(7)
3.38(5)	6.430(4)	18.631(6)	9.636(6)	109.60(6)	1087.48(7)
3.52(5)	6.426(4)	18.620(5)	9.623(4)	109.56(5)	1084.96(8)
3.85(5)	6.418(5)	18.562(6)	9.595(5)	109.55(6)	1077.23(8)
4.04(5)	6.420(5)	18.557(6)	9.583(6)	109.55(6)	1075.86(8)
4.21(5)	6.418(5)	18.544(7)	9.580(6)	109.55(6)	1074.44(9)
Orthorhombic edingtonite					
0.0001	9.5342(6)	9.6445(7)	6.5110(7)	–	598.70(7)
0.81(5)	9.4991(7)	9.5996(10)	6.4866(7)	–	591.50(8)
1.24(5)	9.4696(6)	9.5719(6)	6.4742(7)	–	586.84(6)
1.62(5)	9.4494(5)	9.5517(5)	6.4654(6)	–	583.56(6)
2.18(5)	9.4175(6)	9.5189(7)	6.4519(6)	–	578.38(6)
2.85(5)	9.3804(6)	9.4839(6)	6.4354(6)	–	572.51(6)
3.30(5)	9.3595(4)	9.4643(4)	6.4253(4)	–	569.16(4)
4.25(5)	9.3168(5)	9.4215(6)	6.4044(5)	–	562.17(5)
4.63(5)	9.2996(8)	9.4063(8)	6.3956(9)	–	559.46(8)
5.52(5)	9.2612(6)	9.3680(7)	6.3744(7)	–	553.03(6)
6.00(5)	9.2425(5)	9.3509(5)	6.3636(6)	–	549.97(5)
6.74(5)	9.2106(4)	9.3210(5)	6.3438(6)	–	544.63(5)
Tetragonal edingtonite					
0.0001	9.5911(11)	–	6.5315(17)	–	600.83(21)
0.81(5)	9.5503(10)	–	6.5088(15)	–	593.66(19)
1.24(5)	9.5213(9)	–	6.4958(14)	–	588.87(17)
1.62(5)	9.5007(10)	–	6.4880(16)	–	585.63(18)
2.18(5)	9.4677(9)	–	6.4744(14)	–	580.38(17)
2.85(5)	9.4308(9)	–	6.4604(12)	–	574.60(15)
3.30(5)	9.4089(9)	–	6.4514(13)	–	571.14(16)
4.25(5)	9.3644(9)	–	6.4328(12)	–	564.10(15)
4.63(5)	9.3466(8)	–	6.4258(12)	–	561.35(14)
5.52(5)	9.3080(8)	–	6.4079(11)	–	555.17(13)
6.00(5)	9.2872(8)	–	6.3978(12)	–	551.82(14)
6.74(5)	9.2567(9)	–	6.3818(13)	–	546.84(14)
Thomsonite					
0.0001	13.080(4)	13.056(2)	13.195(2)	–	2253.4(11)
0.31(10)	13.069(1)	13.033(2)	13.194(1)	–	2247.3(3)
1.09(10)	12.985(2)	12.959(2)	13.159(1)	–	2214.2(3)
1.50(10)	12.945(1)	12.910(2)	13.139(1)	–	2195.8(4)
2.17(10)	12.888(2)	12.850(2)	13.110(1)	–	2171.2(4)
3.04(10)	12.814(3)	12.789(5)	13.075(2)	–	2142.5(7)
4.36(10)	12.708(6)	12.683(9)	13.018(3)	–	2098.3(13)
5.25(10)	12.562(6)	12.556(15)	12.985(3)	–	2058.8(20)
6.27(10)	12.562(6)	12.541(4)	12.959(4)	–	2041.5(9)

sured pressure of less than ±0.05 GPa, and with the Equation-of-State (EoS) of quartz (Angel *et al.*, 1997), added as an internal standard (deviation <0.01 GPa). Cell parameters and intensity data were collected at different pressure values in order to calculate the elastic parameters (axial and volume compressibility, unit-strain ellipsoid orientation and magnitude) and to refine the crystal structures. The experiments on the orthorhombic and tetragonal edingtonite show that no phase transition occurs, which may be explained by to an over-hydration effect, even using a nominally penetrating pressure medium. Other experimental details on the single-crystal experiments on scolecite and edingtonite are in Comodi *et al.* (2002) and Gatta *et al.* (2004a and b), respectively.

The H*P*-experiments on a completely ordered potassium gallo-silicate analogue of natrolite, $K_{16}Ga_{16}Si_{24}O_{80}\cdot 12H_2O$, mesolite, scolecite, thomsonite and edingtonite were performed using *in-situ* synchrotron powder diffraction (Lee *et al.,* 2002a, 2004b) using a modified Merrill-Bassett DAC and a nominally penetrating pressure medium (methanol:ethanol:water = 16:3:1). The pressure was calibrated using the ruby fluorescence method (Mao *et al.,* 1986) with deviations in the measured pressure of less than ±0.1 GPa. Natrolite, natrolite type $K_{16}Ga_{16}Si_{24}O_{80}\cdot 12H_2O$, mesolite and scolecite were compressed up to 5 GPa. Between 0.8-1.5 GPa, natrolite, $K_{16}Ga_{16}Si_{24}O_{80}\cdot 12H_2O$ and mesolite showed a pressure-induced volume expansion through the selective sorption of water molecules from the pressure fluid, giving rise to a pressure-induced over-hydration phase (Lee *et al.*, 2002a). The quality of the data only allowed the structural refinement at different pressure values of the natrolite. In addition, only the natrolite cell parameters are reported in the manuscript. The over-hydration effect is reversible for natrolite and mesolite, but appear irreversible for $K_{16}Ga_{16}Si_{24}O_{80}\cdot 12H_2O$ (Lee *et al.*, 2002b). Interesting behaviour was observed for mesolite: the absence of the super-lattice reflections (with $k \neq 3n$) due to the over-hydration effect was observed. Thomsonite and edingtonite were investigated under pressure up to 6.3 GPa. No phase-transition was observed within the pressure range investigated (Lee *et al.*, 2004b), despite the nominally penetrating pressure medium used. The data collected during decompression showed a complete restoration of the lattices. The quality of the diffraction data allowed only cell-parameters least-square refinements; no structural refinement has been reported. A DLS-simulation of the H*P*-crystal structure of thomsonite and edingtonite was performed.

Comparative compressibility

Axial and volume compressibility of natrolite, scolecite, edingtonite (orthorhombic and tetragonal) and thomsonite have previously been calculated using different EoS (or simply by linear regressions) and different weighting schemes for the EoS-fit (using weighed or un-weighed data by the uncertainties in *P* and *V*). In order to compare the elastic parameters of the aforementioned fibrous zeolites, axial and volume compressibility (in terms of "linear" and volume bulk moduli) have been recalculated using a truncated second-order Birch-Murnaghan EoS (Birch, 1947). The Birch-Murnaghan EoS is based upon the assumption that the high-pressure strain of a solid can be expressed as a Taylor series in the Eulerian strain,

$$f = [(V_0/V)^{2/3} - 1] / 2$$

(V_0 and V represent the cell volume, or molar volume, under room and H*P* conditions respectively). Expansion in the Eulerian strain polynomial truncated to second-order has the following form:

$$P = 3/2K_0[(V_0/V)^{7/3} - (V_0/V)^{5/3}],$$

where K_0 represent the bulk modulus ($K_0 = -V_0(\partial P/\partial V)_{P=0} = 1/\beta$; where β is the volume compressibility coefficient). The same Equation of State, as that used to fit the *P-V* data, can be used to describe the axial compressibilities simply by substituting the cube of lattice parameter with the volume (Angel, 2000). In this way, the "linear-K_0" obtained is related to the linear-axial compressibility (β_j) by:

$$\beta_j = -1/(3K_{0j}) = 1/l_{0j}\,(\partial l_j/\partial P),$$

where l_{0j} (j = *a*, *b*, *c*) is the length of the cell axis under room conditions.

Volume and axial compressibility of the quoted FZ were calculated with the EOS-FIT5.2 program (Angel, 2001), adopting the weighted data by the uncertainties in *P* (±0.05 GPa for single-crystal and ±0.10 GPa for powder experiments) and *V* (or *a*, *b*, *c*). Cell parameters are reported in Table 1. Elastic parameters and the EoS-fitting statistic parameters are reported in Table 2. For zeolites investigated using both single-crystal and powder data (*i.e.* scolecite, edingtonite), only the more accurate single-crystal data were used for the EoS-fit.

For natrolite, only two H*P*-data point are available at pressure lower than the phase-transition (at 0.8-1.5 GPa, Table 1). Thus, only the EoS of the over-hydrated H*P*-phase was calculated. Scolecite is the only FZ with a non-orthogonal cell. In order to study the comparative elastic anisotropy, the axial bulk modulus along the vector perpendicular to (001) was also calculated, defined in Table 2 as $K_{csin\beta}$. In this way, the elastic anisotropy along three mutually orthogonal directions can be described. Note that for scolecite, the Si/Al-framework in the monoclinic *C*-centered lattice shows the SBU-chains along the *a*-axis (Comodi *et al.*, 2002). Volume EoS-fits of the aforementioned FZ are shown in Fig. 3. For thomsonite, the experimental V_0 leads to an evident misfit between observed data points at low-pressure and the EoS (Fig. 3). A second EoS-fit has been determined using all the volume data but *without* the experimental V_0. In this case, the new EoS-fit improves significantly, as shown in Fig. 3 and Table 2. As reported by Angel (2000) and Gatta *et al.* (2004b), the effect of the uncertainty in V_0 on the compression parameters is very strong and can often lead to elastic parameters that are completely wrong. The last consideration is extremely important for zeolites, where the V_0 value is dependent on variation in experimental conditions, such as humidity (Fridriksson *et al.*, 2003; Gatta *et al.*, 2004b; Lee *et al.*, 2004b and c).

Eulerian strain *vs* "normalised pressures" plots (*fe-Fe* plot, Angel, 2000) for natrolite, scoelcite, edingtonite and

Table 2. Elastic parameters of H*P*-natrolite, scolecite, orthorhombic-tetragonal edingtonite and thomsonite. Second-order BMEoS-fitting statistical parameters are also reported (see Angel, 2001, for details).

	Natrolite (high-*P*)	Scolecite	Orthorhombic edingtonite	Tetragonal edingtonite	Thomsonite
Space group	*Fdd*2	*Cc*	$P\,2_12_12$	$P2_1m$	*Pncn*
a_0 (Å)	18.655(23)	6.531(1)	9.5349(9)	9.592(1)	13.089(11)
K_a (GPa)	33(2)	66(2)	53.2(4)	51.0(3)	38(2)
b_0 (Å)	19.129(23)	19.034(6)	9.6440(8)	–	13.057(3)
K_b (GPa)	30(1)	46(1)	53.2(3)		41(1)
c_0 (Å)	6.576(2)	9.827(4)	6.5108(8)	6.528(1)	13.199(2)
K_c (GPa)	112(5)	48(1)	75.9(8)	87(1)	99(2)
$c_0$senβ (Å)		9.236(3)			
$K_{csin\beta}$ (GPa)		55(2)			
K_a:K_b:K_c	1.10:1.00:3.73	1.43:1.00:1.04	1.00:1.00:1.43	1.00:1.00:1.71	1.00:1.08:2.60
K_a:K_b:$K_{csin\beta}$		1.43:1.00:1.19			
V_0 (Å^3)	2343(6)	1148.76(8)	598.71(7)	600.9(2)	2245.4(2)
					*2262(3)
K_{T0} (GPa)	43(2)	54.6(6)	59.3(2)	59.3(4)	55(1)
					*49(1)
Fe(0) (GPa)	43(4)	56(2)	59(1)	59(1)	57(2)
					*48(1)
Fitting statistic parameters					
χ^2_w	0.7474	4.8100	0.5182	0.3846	6.544
					*1.518
Rw %	2.161	3.747	0.860	0.789	7.310
					*3.218
$\lvert P_{obs}$-$P_{cal}\rvert_{max}$ (GPa)	0.105	0.253	0.075	0.077	0.415
					*0.303

*Parameters calculated using the V_0 value obtained from a second-order Birch-Murnaghan EoS *without* the observed V_0 at room pressure (see text).

thomsonite are reported in Fig. 4 and the weighted linear regressions, through the data, are shown. For all the zeolites investigated, the calculated *Fe*(0) values are in excellent agreement with the K_{T0} values obtained by the EoS-fit (Table 2). The almost horizontal weighted linear regression justifies the second-order BM-EoS used (Angel, 2000) for all the FZ.

The structural analogy among the FZ group induces similar elastic behaviour and a "FZ-average bulk modulus" can be calculated: K_{T0}(FZ) = 50±10 GPa. The end-members of this group are represented by natrolite (K_{T0} = 43(4) GPa) and edingtonite (K_{T0} = 59(1) GPa). The FZ-average bulk modulus value is larger than the other non-FZ bulk moduli (K_{T0}(heulandite) = 27.5(2)GPa, Comodi *et al.*, 2001; K_{T0}(bikitaite) = 44.2(4)GPa, Comodi *et al.*, 2003; K_{T0}(bikitaite) = 45(1) GPa, Ferro *et al.*, 2002; K_{T0}(ZEO-A) = 22.1(3) GPa, Arletti *et al.*, 2003)

The elastic anisotropy is reported in Table 2 as a ratio between the axial bulk moduli. It is evident that for all the FZ a similar elastic response on the plane perpendicular to the SBU-chains, represented by two similar axial compressibilities, exists. In contrast, the compressibility along the chains appears to be significantly different.

P-induced structural evolution

The H*P*-structural behaviour of fibrous zeolites can be studied by comparing the structural refinements carried out at different pressures. Structural data are available for natrolite (Lee *et al.*, 2002a), scolecite (Comodi *et al.*, 2002) and orthorhombic-tetragonal edingtonite (Gatta *et al.*, 2004a and b).

All the FZ show that the pressure increase does not produce any relevant variation on the tetrahedra: T-O bond distances and O-T-O angles are slightly modified in response of the applied pressure. In contrast, the polyhedral tilting basically drives the main deformation mechanisms, which produces inter-tetrahedral angle variations. The main deformation mechanism, observed under pressure for all the FZ, is represented by a cooperative rotation of the SBU along the chain-axis (Fig. 5). As noted by Comodi *et al.* (2002) and Gatta *et al.* (2004a and b), the acute angles of the channel decrease and, in contrast, the obtuse angles increase. As a consequence, the short "free diameter" (Baerlocher *et al.*, 2001) of the channel decreases and, in contrast, the long free diameter increases (Fig. 4). In other words, there is an increase of the pore ellipticity with pressure. A supplementary way to quantify the effect of the SBU-chains anti-rotation was introduced by Comodi *et al.* (2002) defining the „φ angle" (Fig. 4). The φ angle value increases with increasing pressure, as shown for scolecite (Comodi *et al.*, 2002), orthorhombic and tetragonal edingtonite (Gatta *et al.*, 2004b). The same mechanism can be deduced from the structural refinement of low-*P* phase and high-*P* over-hydrated phase of natrolite (Lee *et al.*, 2002a).

At first approximation, the SBU appear to act as "rigid-units" only. In fact, the tetrahedral tilting induces a change of the SBU size. Comodi *et al.* (2002) and Gatta *et al.*

(2004a) calculated SBU volume variation with pressure for scolecite and tetragonal edingtonite, respectively. The volume was calculated considering the SBU as a distorted polyhedron with six vertices represented by the tetrahedral sites. The bulk moduli, obtained by weighted linear regressions, are 96(6) and 97(8) GPa for scolecite and tetragonal edingtonite, respectively. In order to investigate the effect of the Si/Al-distribution on the elastic behaviour of the tetrahedral framework, Gatta *et al.* (2004b) calculated the SBU-bulk moduli for both orthorhombic and tetragonal edingtonite. In this case, SBU volumes at different pressures were calculated considering the building unit as being completely contained in a prism of rhombic section, delimited by the four oxygen atoms, and with the height represented by the distances between the apical tetrahedra (T1-T1 or Si1-Si1). The two SBU bulk moduli, calculated from a weighted linear regression, are 125(8) and 111(4) GPa for orthorhombic and tetragonal edingtonite, respectively. The slightly different results obtained by Gatta *et al.* (2004a) and Gatta *et al.* (2004b) for the tetragonal edingtonite (97(8) *vs* 114(4) GPa, respectively) may be attributed to the different methods adopted for the volume calculation. However, it is possible to infer that the SBU of FZ show a bulk modulus of approximately 110±15 GPa.

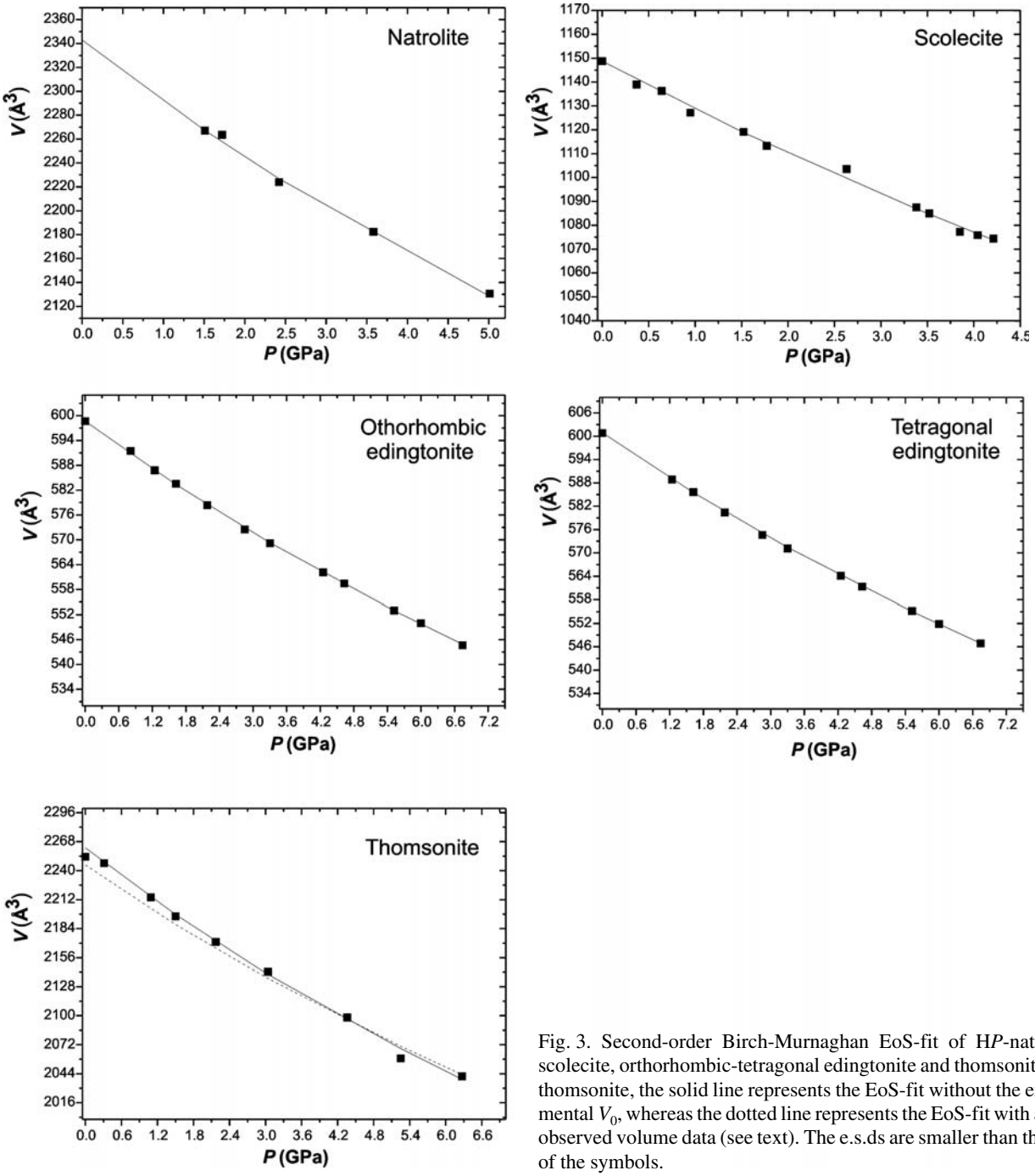

Fig. 3. Second-order Birch-Murnaghan EoS-fit of H*P*-natrolite, scolecite, orthorhombic-tetragonal edingtonite and thomsonite. For thomsonite, the solid line represents the EoS-fit without the experimental V_0, whereas the dotted line represents the EoS-fit with all the observed volume data (see text). The e.s.ds are smaller than the size of the symbols.

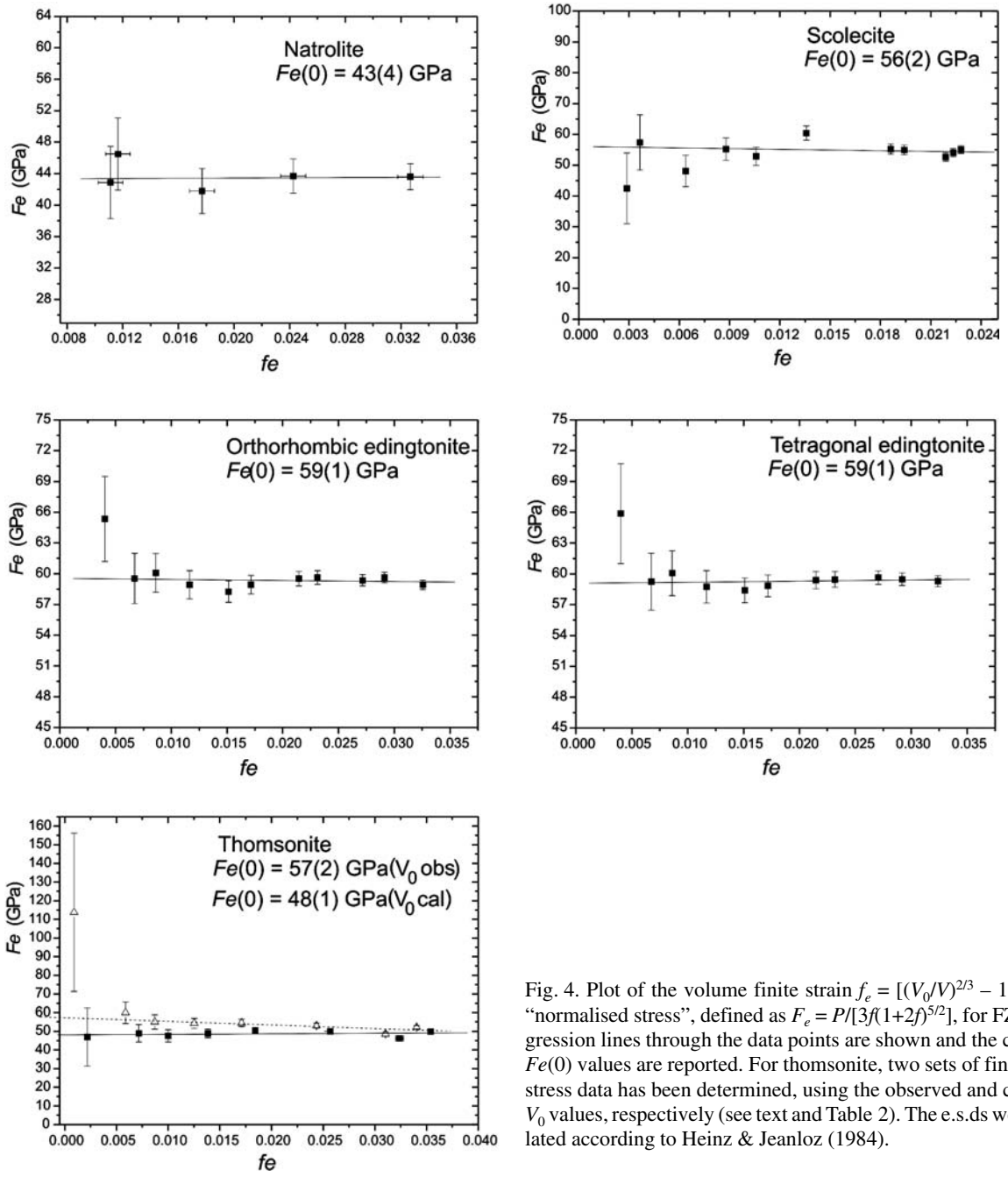

Fig. 4. Plot of the volume finite strain $f_e = [(V_0/V)^{2/3} - 1]/2$ *vs* the "normalised stress", defined as $F_e = P/[3f(1+2f)^{5/2}]$, for FZ. The regression lines through the data points are shown and the calculated $Fe(0)$ values are reported. For thomsonite, two sets of finite strain-stress data has been determined, using the observed and calculated V_0 values, respectively (see text and Table 2). The e.s.ds were calculated according to Heinz & Jeanloz (1984).

The cooperative anti-rotation mechanism of the SBU reduces the free volume of the 8-membered ring channels along the chain-axis. Comodi *et al.* (2002) and Gatta *et al.* (2004a) calculated the bulk modulus of the 8-membered ring channel, running along the chain-axis, for scolecite ($K_{[100]ch} = 17(2)$) and tetragonal edingtonite ($K_{[001]ch} = 19(1)$ GPa), respectively.

Using a non-penetrating pressure transmitting medium, the extra-framework content of FZ is not affected by strong modification in response of the applied pressure: the coordination numbers appear unchanged, the bond angles and the bond distances are only slightly modified (Lee *et al.*, 2002a; Comodi *et al.*, 2003; Gatta *et al.*, 2004a and 2004b). Gatta *et al.* (2003a) and Gatta *et al.* (2004a) calculated the bulk moduli of the Ca-polyhedron (coordination number – CN: 7) and the Ba-polyhedron (CN: 10) belonging to scolecite and edingtonite, respectively. The Ca-polyhedron shows a K_{T0} value of 73(5), whereas the bulk modulus of the Ba-polyhedron is $K_{T0} = 72(5)$ GPa.

Using a penetrating pressure medium, Lee *et al.* (2002a) showed an over-hydration effect in natrolite at 0.8-1.5 GPa. Just before the phase-transition (at 0.8 GPa), four framework oxygen atoms and two H_2O-molecules coordinate with the Na site. At 1.51 GPa, a new water molecule site has been observed. As a consequence, a change in the topological configuration of the Na-polyhedron occurs: the coordination number increases to seven, four framework oxygens and two water molecules sites. Due to the over-hydration ef-

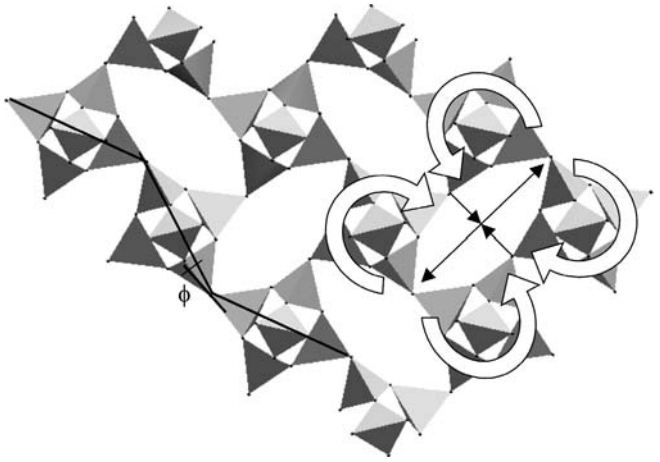

Fig. 5. Main deformation mechanism of fibrous zeolite framework under pressure: SBU-cooperative anti-rotation mechanism and *P*-induced effects on the [001]-channel free diameters.

fect, the chemical formula of natrolite changes from $Na_{16}Al_{16}Si_{24}O_{80}{\cdot}16H_2O$ to $Na_{16}Al_{16}Si_{24}O_{80}{\cdot}32H_2O$, without any modification of the structural symmetry. As stated by Lee *et al.* (2002a) and Lee *et al.* (2004a), the super-hydrated phase contains hydrogen-bonded helical water nanotubes along the *c*-axis. This provides the opportunity to study the dynamics of confined water at the nanoscale by *P*-experiments. The *P*-induced over-hydration effect was also observed for natrolite (Belitsky *et al.*, 1992) and scolecite (Bazhan *et al.*, 1997) using Raman spectroscopy. In contrast, the large Ba-polyhedra, which lie in the channels of edingtonite, do not allow any *P*-induced over-hydration effect, as confirmed by Goryainov *et al.* (2003) with Raman spectroscopy up to 6 GPa and by Gatta *et al.* (2004b) by means of single-crystal diffraction data. It is still unclear why thomsonite does not show any over-hydration effect (Lee *et al.*, 2004b), considering the structural homologies with natrolite and scolecite. However, Lee *et al.* (2004b) provided a possible explanation: thomsonite already contains more water molecules at ambient conditions than natrolite; therefore *P*-induced over-hydration does not likely occur in thomsonite.

Discussion

Elastic parameters of natrolite, scolecite, orthorhombic-tetragonal edingtonite and thomsonite allow us to understand the role played by the Si/Al-ordering, by the different cross-linking of the SBU-chains and by the extra-framework content on the *P*-behaviour of the FZ.

Natrolite and scolecite are characterised by the same framework type (NAT) and they show an almost fully ordered Si/Al-distribution. Thus, the different bulk modulus values (K_{T0} natr. = 43(2) GPa, K_{T0} scol. = 54.6(6) GPa) can only be attributed to the different extra-framework content. The isomorphic orthorhombic and tetragonal edingtonite (EDI) show the same bulk modulus value (59.3(2), 59.3(4) GPa, respectively). In other words, the Si/Al-distribution does not influence the lattice compressibility, even though the SBU-bulk moduli appear to be slightly different (O-eding.: 125(8) GPa; T-eding.: 111(4) GPa). This means that the pores and the extra-framework content accommodate the slightly different elastic behaviour of the SBU, leading to an equal bulk modulus value calculated on the basis of the cell-volume variation. The bulk modulus of thomsonite (THO) is included between those of natrolite and scolecite (Table 2). This is reasonable considering that, as already stated, the crystal structure of thomsonite accommodates both Na and Ca as extra-framework cations, showing similarities with both natrolite and scolecite crystal structures. The bulk modulus values of FZ appear to be related to the nature of the extra-framework cations. In general, Na-FZ are more compressible than (Na+Ca)- or Ca-FZ, which are more compressible that Ba-FZ. However, a simple relationship between ionic radius and bulk modulus could not have a robust physical basis, because the topological configuration of the extra-framework content in the channels is completely different (*i.e. two* Na-polyhedra with CN = 7 in H*P*-natrolite; *one* Ca-polyhedra with CN = 7 in scolecite; *one* Ba-polyhedra with CN = 10 in edingtonite). Since there are no FZ with the same extra-framework content but different cross-linking of the SBU-chains, the role of the linking geometry on the bulk modulus cannot be defined.

All the FZ investigated show an almost isotropic elastic behaviour on the plane perpendicular to the SBU-chain. The differences between the normalised axial bulk moduli (K_a:K_b:K_c) along the two orthogonal directions perpendicular to the SBU-chains axis are less than 19% (Table 2). This difference is less than 10% if we do not consider the (monoclinic) scolecite. However, as shown in Table 2, the differences of the elastic response along the SUB-chains axis with respect to the two perpendicular directions are strongly different among the FZ. In addition, the absolute values of the axial bulk moduli are completely different (Table 2). Elastic data of the isomorphic orthorhombic and tetragonal edingtonite confirm that the Si/Al-distribution influences the elastic anisotropy. In addition, data of natrolite and scolecite suggest that the extra-framework content also plays a relevant role on the elastic anisotropy. The different topological configuration of the Na and Ca-polyhedron and the different orientation of the Na/Ca-O vectors would make such polyhedra differently anisotropic, influencing the lattice anisotropy.

The structural evolution of FZ appears to be basically driven by one main deformation mechanism: the cooperative anti-rotation of the SBU (Fig. 5). This mechanism is independent of the nature of extra-framework content, of the SBU-chains cross-linking geometry and of the Si/Al-distribution.

The H*T*-behaviour of FZ has been extensively investigated (Van Reeuwijk, 1972; Peacor, 1973; Alberti & Vezzalini, 1983; Gottardi & Galli, 1985; Ståhl & Hanson, 1994 and 1998). All the FZ show a continuous loss of water with increasing temperature up to the amorphization. The H*T*-structural data available in the literature show that the water loss induces the same deformation mechanism observed under pressure conditions: the cooperative anti-rotation of the SBU. In this case, the mechanism is driven by the water loss, with the consequent reduction in volume of the micro-pores. However, when a non-penetrating *P*-medium is used, the structural modifications induced by pressure are less dramatic than those induced by *T*. In fact, the crystal structure

of FZ is preserved at least up to 5-6 GPa and the cell parameters measured during decompression, or the structural refinements performed at room condition after decompression, show an almost complete restoration of the crystal structures (Comodi *et al.*, 2002; Gatta *et al.* 2004a, 2004b). Only two studies have been devoted to the complete amorphization of FZ using a non-penetrating *P*-medium, showing that natrolite (Goryainov, 2004) and scolecite (Gillet *et al.*, 1996) become irreversibly amorphous at P>10-12 GPa.

Conclusions

The elastic data of FZ here re-elaborated allow a comparative study of the isothermal behaviour under H*P*-condition. Some general considerations may be made:

1) All the FZ show the same *P*-induced main deformation mechanism, represented by the cooperative rotation (anti-rotation) of the SBU around the chain-axis (Fig. 5). This mechanism reduces the free volume of the 8-membered ring channels and is independent of the nature of extra-framework content, of the SBU-chains cross-linking geometry and of the Si/Al-distribution;

2) In agreement with Gatta *et al.* (2003b), this comparative study basically confirms that the compressibility of zeolites is not directly related to the microporosity, which can be represented by the framework density (FD, Baerlocher *et al.*, 2001). In fact, the bulk moduli of the FZ are different even though their FD is similar;

3) The role of the extra-framework content on the FZ-lattice compressibility and on the elastic anisotropy can be inferred. The bulk modulus value changes in response to the extra-framework content, following the sequence: K_{T0}(Ba-FZ)>K_{T0}(Ca-FZ)>K_{T0}(Ca+Na FZ)>K_{T0}(Na-FZ);

4) As shown by the experimental data of isomorphic orthorhombic and tetragonal edingtonite, the Si/Al-distribution can influence the elastic behaviour of the framework, represented by the SBU-bulk modulus. This effect is evident on the lattice anisotropy, but is not strong enough to be reflected on the lattice compressibility;

5) The elastic anisotropy is influenced by the topological symmetry of the framework, as reflected by the similar compressibility on the plane perpendicular to the SBU-chains. Moreover, the Si/Al-distribution and the extra-framework content influence the absolute values of the axial compressibilities (Table 2).

6) No evidence of the role played by the SBU-chains cross-linking on the FZ-elastic behaviour has at present been found.

Acknowledgements: Thanks are due to the Associated Editor E. Passaglia and to J.M. Malézieux and Y. Lee for their helpful suggestions.

References

Alberti, A. & Vezzalini, G. (1981): A partially disordered natrolite: relationships between cell parameters and Si-Al distribution. *Acta Cryst.*, **B37**, 781-788.

–,– (1983): How the structure of natrolite is modified through the heating induced dehydration. *N.Jb. Miner. Mh.*, **1983**, 135-144.

Alberti, A., Vezzalini, G., Tazzoli, V. (1981): Thomsonite: a detailed refinement with cross checking crystal energy calculations. *Zeolites*, **1**, 91-97.

Allan, D.R., Miletich, R., Angel, R.J. (1996): A diamond-anvil cell for single-crystal X-ray diffraction studies to pressures in excess of 10 GPa. *Rev. Sci. Instrum.*, **67**, 840-842.

Angel, R.J. (2000): Equation of State. *in* "High-Temperature and High-Pressure Crystal Chemistry", Hazen, R.M. and Downs, R.T., eds. Review in Mineralogy and Geochemistry, Vol. 41, pp. 35-59, Mineralogical Society of America and Geochemical Society, Washington, DC.

– (2001): EOS-FIT V6.0. Computer program. Crystallography Laboratory, Dept. Geological Sciences, Virginia Tech, Blacksburg, U.S.A.

Angel, R.J., Allan, D.R., Miletich, R., Finger, L.W. (1997): The use of quartz as an internal pressure standard in high-pressure crystallography. *J. Appl. Cryst.*, **30**, 461-466.

Armbruster, T. & Gunter, M.E. (2001): Crystal structures of natural zeolites. *in* "Natural zeolites: occurrence, properties, application", Bish, D.L. and Ming, D.W., eds. Review in Mineralogy and Geochemistry, Vol. 45, pp. 1-57, Mineralogical Society of America and Geochemical Society, Washington, DC.

Artioli, G., Smith, J.V., Kvick, Å. (1984): Neutron diffraction study of natrolite, $Na_2Al_2Si_3O_{10}\,2H_2O$, at 20 K. *Acta Cryst.*, **C40**, 1658-1662.

Artioli, G., Smith, J.V., Pluth, J.J. (1986): X-ray structural refinement of mesolite. *Acta Cryst.*, **C42**, 937-942.

Baerlocher, Ch., Meier, W.M., Olson, D.H. (2001): Atlas of zeolite framework types, 5th edn, Elsevier, Amsterdam, NL, 302 pp.

Ballone, P., Quartieri, S., Sani, A., Vezzalini, G. (2002): High-pressure deformation mechanism in scolecite: A combined computational-experimental study. *Am. Mineral.*, **87**, 1194-1206.

Bazhan, I.S., Fursenko, B.A., Kholdeev, O.V. (1997): Scolecite phase transformation at high hydrostatic pressure. *in* "Proc. 5th Int. Conference on the Occurrence, Properties and Utilization of Natural Zeolites", Ischia, Italy, 57-59.

Belitsky, I.A., Fursenko, B.A., Gabuda, S.P., Kholdeev, O.V., Seryotkin, Y.V. (1992): Structural transformation in Natrolite and Edingtonite. *Phys. Chem. Minerals*, **18**, 497-505.

Birch, F. (1947): Finite elastic strain of cubic crystal. *Phys. Rev.*, **71**, 809-824.

Bish, D.L., Vaniman, D.T., Chipera, S.J., Carey, J.W. (2003): The distribution of zeolites and their effects on the performance of a nuclear waste repository at Yucca Mountain, Nevada, U.S.A. *Am. Mineral.*, **88**, 1889-1902.

Comodi, P. & Zanazzi, P.F. (1993): Improved calibration curve for the Sm^{2+}: BaFCl pressure sensor. *J. Appl. Cryst.*, **26**, 843-845.

Comodi, P., Gatta, G.D., Zanazzi, P.F. (2001): High-pressure structural behavior of heulandite. *Eur. J. Mineral.*, **13**, 497-505.

–,–,– (2002): High-pressure behavior of scolecite. *Eur. J. Mineral.*, **14**, 567-574.

–,–,– (2003): Effects of pressure on the structure of bikitaite. *Eur. J. Mineral.*, **15**, 247-225.

Davis, M.E. (2002): Ordered porous materials for emerging applications. *Nature*, **417**, 813-821.

Fälth, L. & Hansen, S. (1979): Structure of scolecite from Poona, India. *Acta Cryst.*, **B35**, 1877-1880.

Ferro, O., Quartieri, S., Vezzalini, G., Fois, E., Gamba, A., Tabacchi, G. (2002): High-pressure behaviour of bikitaite: An integrated theoretical and experimental approach. *Am. Mineral.*, **87**, 1415-1425.

Fridriksson, T., Bish, D.L., Bird, D.K. (2003): Hydrogen-bonded water in laumontite I: X-ray powder diffraction study of water site occupancy and structural changes in laumontite during room-temperature isothermal hydration/dehydration. *Am. Mineral*., **88**, 277-287.

Galli, E. (1976): Crystal structure refinement of edingtonite. *Acta Cryst.,* **B32,** 1623-1627.

Gatta, G.D. & Boffa Ballaran, T. (2004): New insight into the crystal structure of orthorhombic edingtonite. *Min. Mag*., **68**, 167-175.

Gatta, G.D., Boffa Ballaran, T., Comodi, P., Zanazzi, P.F. (2003a): Topological effects on microporous materials under pressure conditions: framework and extra-framework behaviour of Ca- and Ba-fibrous zeolites. *in* "Proc. 32nd Congress of Italian Association of Crystallography", Trieste, Italy.

Gatta, G.D., Comodi, P., Zanazzi, P.F. (2003b): New insights on high-pressure behaviour of microporous materials from X-ray single-crystal data. *Micr. Mes. Materials*, **61**, 105-115.

Gatta, G.D., Boffa Ballaran, T., Comodi, P., Zanazzi, P.F. (2004a): Isothermal equation of state and compressional behaviour of tetragonal edingtonite. *Am. Mineral.,* **89**, 633-639.

–,–,–,– (2004b): Comparative compressibility and equation of state of orthorhombic and tetragonal edingtonite. *Phys. Chem. Minerals*, **31**, 288-298.

Gillet, P., Malézieux, J.M., Itié, J.P. (1996): Phase changes and amorphization of zeolites at high pressure: The case of scolecite and mesolite. *Am. Mineral*., **81**, 651-657.

Goryainov, S.V. (2004): Amorphization of natrolite at high-pressure. *in* "Proc.10th EMPG", Frankfurt, Germany. *Lithos*, **73**, S45.

Goryainov, S.V., Kursonov, A.V., Miroshnichenko, Yu.M., Smirnov, M.B., Kabanov, I.S. (2003): Low-temperature anomalies of infrared band intensities and high-pressure behaviour of edingtonite. *Micr. Mes. Maerials*, **61**, 283-289

Gottardi, G. & Galli, E. (1985): Natural Zeolites. Springer-Verlag, Berlin, Germany, 409 pp.

Heinz, D.L. & Jeanloz, R. (1984): The equation of state of the gold calibration standard. *J. Appl. Phys*., **55**, 885-893.

Kallo, D. (2001): Applications of natural zeolites in water and wastewater treatment. *in* "Natural zeolites: occurrence, properties, application", Bish, D.L. and Ming, D.W., eds. Review in Mineralogy and Geochemistry, Vol. 45, pp. 519-550, Mineralogical Society of America and Geochemical Society, Washington, DC.

Krogh Andersen, E., Krogh Andersen, I.G., Ploug-Sorensen, G. (1990): Disorder in natrolites: structure determinations of three disordered natrolites and one lithium-exchanged disordered natrolite. *Eur. J. Mineral.*, **2**, 799-807.

Li, H., Laine, A., O'Keeffe, M., Yaghi, O.M. (1999): Supertetrahedral sulphide crystals with giant cavities and channels. *Science*, **283**, 1145-1147

Lee, Y., Vogt, T., Hriljac, J.A., Parise, J.B., Artioli, G. (2002a): Pressure-Induced Volume Expansion of Zeolites in the Natrolite Family. *J. Am. Chem. Soc*., **124**, 5466-5475.

Lee, Y., Vogt, T., Hriljac, J.A., Parise, J.B., Hanson, J.C., Kimk, S.J. (2002b): Non-framework cation migration and irreversible pressure-induced hydration in a zeolite. *Nature,* **420**, 485-489.

Lee, Y., Martin, D., Parise, J.B., Hriljac, J.A., Vogt, T. (2004a): Formation and manipulation of confined water wires. *Nanoletters*, **4**, 619-621.

Lee, Y., Hriljac, J.A., Studer, A., Vogt, T. (2004b): Anisotropic compression of edingtonite and thomsonite to 6 GPa at room temperature. *Phys. Chem. Minerals*, **31**, 22-27

Lee, Y., Hriljac, J.A., Vogt, T. (2004c): Pressure-induced migration of zeolitic water in laumontite. *Phys. Chem. Minerals*, **31**, 421-428.

Mao, H.K., Xu, J., Bell, P.M. (1986): Calibration of the ruby pressure gauge to 800 kbar under quasi-hydrostatic conditions. *J. Geophys. Res*., **91**, 4673-4676.

Mazzi, F., Galli, E., Gottardi, G. (1984): Crystal structure refinement of two tetragonal edingtonites. *N. Jb. Miner. Mh*., **1984**, 373-382.

Merrill, L. & Bassett, W.A. (1974): Miniature diamond anvil pressure cell for single-crystal X-ray diffraction studies. *Rev. Sci. Instrum*., **45,** 290-294.

Passaglia, E. & Sheppard, R.A. (2001): The crystal chemistry of zeolites. *in* "Natural zeolites: occurrence, properties, application", Bish, D.L. and Ming, D.W., eds. Review in Mineralogy and Geochemistry, Vol. 45, pp. 69-116, Mineralogical Society of America and Geochemical Society, Washington, DC.

Peacor, D.R. (1973): High-temperature, single-crystal x-ray study of natrolite. *Am. Mineral*., **58**, 676-680.

Smith, J.V. (1983): Enumeration of 4-connected 3-dimensional nets and classification of framework silicates: combination of 4-1 chain and 2D nets. *Z. Kristallogr.*, **165**, 191-198.

Ståhl, K. & Hanson, J. (1994): Real-time X-ray synchrotron powder diffraction studies of the dehydration processes in scolecite and mesolite. *J. Appl. Cryst.*, **27**, 543-550.

–,– (1998): An in situ study of the edingtonite dehydration process from X-ray synchrotron powder diffraction. *Eur. J. Mineral*., **10**, 221-228.

Ståhl, K., Kvick, Å., Smith, J.V. (1990) Thomsonite, a neutron diffraction study at 13 K. *Acta Cryst*., **C46**, 1370-1373

Stuckenschmidt, E. & Kirfel, A. (2000): Zeolites of NAT topology: structure refinement of mesolite from single crystal X-ray data and comparison with the structures of natrolite and scolecite. *Eur. J. Mineral*., **12**, 571-579

Tchernev, D.I. (2001): Natural zeolites in solar energy, heating, cooling, and energy storage. *in* "Natural zeolites: occurrence, properties, application", Bish, D.L. and Ming, D.W., eds. Review in Mineralogy and Geochemistry, Vol. 45, pp. 589-618, Mineralogical Society of America and Geochemical Society, Washington, DC.

Van Reeuwijk, L.P. (1972): High temperature phases of zeolites of the natrolite group. *Am. Mineral*., **57**, 499-510.

Zheng, N., Bu, X., Feng, P. (2002): Microporous and photoluminescent chalcogenide zeolite analog. *Science*, **298**, 2366-2369

–,–,– (2003): Synthetic design of crystalline inorganic chalcogenides exhibiting fast-ion conductivity. *Nature*, **426**, 428-432.

Received 4 October 2004
Modified version received 27 December 2004
Accepted 24 January 2005